OPTIMIZATION DESIGN OF ALU FOAM-FILLED S-SHAPE SQUARE TUBE UNDER AXIAL DYNAMIC LOADING

NGUYEN VAN SY, NGUYEN THANH TAM
Industrial University of Ho Chi Minh City
nguyenvansy@iuh.edu.vn

Abstract. This paper presents finite element simulation of the crash behavior and the energy absorption characteristics of S-shape square tubes which were fully or partially filled with aluminum foams. Base on the numerical results, it is found that, the density, the length of the filled foam and the thickness of tube directly affect the specific energy absorption (SEA) and peak crushing force (PCF) of the S-shape tubes. In this paper, the multi-objective particle swarm optimization (MOPSO) algorithm is employed to seek for optimal designs for the partial foam-filled S-shape tubes (PFSTs) and the full foam-filled S-shape tubes (FFSTs) with various design parameters such as the density, the length of filled foam and the thickness of tube, where response surface models are established to formulation SEA and PCF. The optimization results showed the energy absorption capability per unit mass of the PFSTs is more powerful than that of the FFSTs while the PCF constrained under the same level.

Keywords. S-shape tube; Full foam-filled; Partial foam-filled; Crashworthiness; Multiobjective optimization; Finite element method.

1 INTRODUCTION

The front and rear side rails usually have an S-shape to avoid interference with other components such as engine, drive train, fuel tank, and etc. These members play the most important role in absorbing, which is the main energy absorption components in the case of frontal or rear collision, and it directly affects the energy absorption characteristics of the passenger car [1]. Therefore, it is very important to study the crashworthiness characteristics of the thin-walled front and rear side rails. In this context, K. Abolfazl [2] and C. Kefang [3] studied on the collapse behavior of S-shaped beams by using numerical and experimental methods. It can be found that the reinforcement of the cross-section can improve the specific energy absorption of the S-shaped longitudinal beam during impact. On the other hand, Kim et al. [4], carried out simulation studies on the design aspect of a front side rail structure of an automobile body and investigated several internal stiffeners to strengthen the longitudinal tubes. Various orientations of cross-section and methods of internal strengthening are investigated using the inner stiffening member or filling fully sections with aluminum foam. Zhang and Saigal [5] presented crushing behavior of a 3D S-shape aluminum square frame under an axial loading. Different cross-section reinforcements and aluminum foam-filled reinforcement have also discussed. They showed that, the left diagonal reinforced structure has the highest specific energy absorption. Most recently, Ahmed et. al [6] presented finite element simulations of the crash behavior and the energy absorption characteristics of thin S-shaped longitudinal members with variable cross-sections made of different materials to investigate the design of optimized energy-absorbing members. The results showed that an octagonal cross-section with vertical diagonal inner stiffeners provide a good combination of structural reinforcements to increase the bending resistance of the members.

Relating to foam-filled thin-walled structures, many researchers had done a lot of work on studying the energy absorption characteristics of foam-filled thin-walled structures by using experimental, analytical and numerical methods during the past decades. Foam-filled thin-walled structures can absorb more impacting energy than the corresponding non-filled thin-walled structures without in creasing too much total weight [7]. The foam-filler can not only provide the advantage of weight efficiency, but also increases the efficiency of the structure due to the contact between the side-wall and the foam-filler. In addition, it can be found that the energy absorption capacity of foam-filled thin-walled structures is mainly determined by the parameters of thin wall geometry and foam density when the loading condition

is fixed. Although foam-filled thin-walled tubes are able to enhance the energy absorption capacity, the energy absorption was found to be highly dependent on the foam density, where the higher foam density, the higher energy absorption. In another study, Reyes et al. [8] found that high-density aluminum foam could increase the energy absorption of thin-walled square tube considerably, but the specific energy absorption can be lowered compared with the empty tube. In addition, the addition of aluminum foam-filled structures increased the energy absorption but also led to an increase in peak force. Chen et al. [9] carried out experimental and numerical studies on the bending collapse of thin-walled beams filled partially or fully aluminum foam. They showed that, partially filling offers significant reduction of foam weight while maintaining higher crushing resistance.

Base on the above investigations, it is necessary to optimize the crashworthiness of the foam-filled S-shape tubes by seeking for the optimal thickness, length of foam-fill and foam-fill density. In optimization regard, Zarei and Kroger [10,11] implemented the multi-criteria design optimization procedure to maximum the energy absorption and minimum the weight of foam-filled aluminum tubes. Hou et al. [12,13] developed a multi-objective optimization frame work for optimizing thin-walled column filled with aluminum foam. In their optimization process, surrogate model techniques were used in order to reduce the computation cost. Bietal. [14] optimized single and triple-cell hexagonal columns filled with aluminum foams aiming at maximum SEA with the constraint of mean crushing force. Zhang et al. [15] optimized the crashworthiness of foam-filled bitable square column using the Kriging meta-modeling technique as well as the genetic algorithm and non-dominated sorting genetic algorithm II (NSGAII).

In this paper, the energy absorption characteristics of the PFSTs and FFSTs are firstly investigated by nonlinear finite element analysis through LS-DYNA. Then, the PFSTs and FFSTs are optimized by adopting MOPSO algorithm to achieve maximum SEA and minimum PCF. During the MOD process, the response surface method (RSM) is utilized to formulate the complex design problem. The optimal designs of PFST that may provide an extremely excellent crashworthiness performance can be obtained.

2 PROBLEM DESCRIPTION

2.1 Structures of the crushing analysis

The structure considered in this study is the thin-walled S-shape tube with a square cross-section with fully or partially aluminum foam-filling. The model can represent a highly idealized front side rail of a car. It is also shown in figure 1 that the sectional dimension of frame is 80x80 mm. The length of the straight end part is 200 mm. The S-shape is composed of two circular arches in both the X plane and Y plane [5]. The detailed dimensions are given in figure 1(a).

One end of the model is impacted onto a rigid wall, and the load of 500 kg is applied on the other end as an initial velocity of 11 m/s boundary condition in the Z-direction. All the degrees of freedom except for Z translation are fixed on the moving end to model the actual deformation of the front side rail of a car under frontal collision. Because the geometry of the model is S-shaped, the member will be subjected to a combination of axial compression, bending and torsion moment. Therefore, from the point of view of loading, the above model corresponds well to a real front rail of a passenger car figure. 1(b).

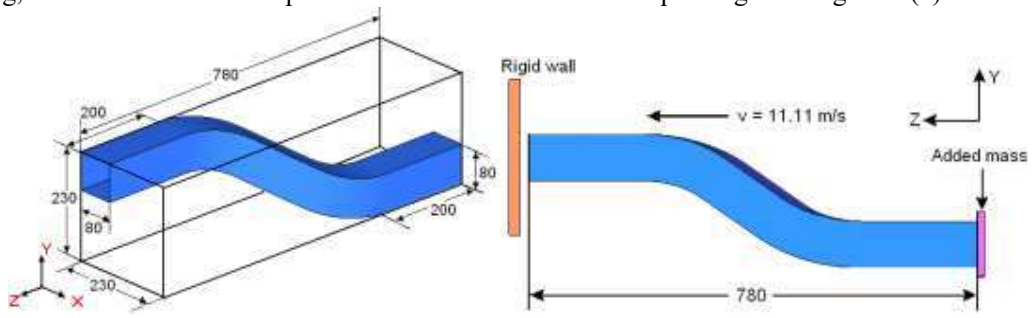

(a) (b)

Figure 1 (a) S-shape tube (the unit of measure is mm), (b) loading condition.

2.2 Structural crashworthiness indicators

In order to evaluate the crashworthiness of the thin-walled structures, it is essential to define the crashworthiness indices. Energy absorption (EA), SEA and PCF are usually used as the important indicators for evaluating the crashworthiness. The energy absorption of a structure subjected to the axial loading can be expressed as:

$$\mathrm{EA(d)} = \int_0^d P.\delta d \tag{1}$$

where d is the axial crushing distance and P denotes the axial crushing force. The specific energy absorption is defined as the ratio of the absorbed energy to the mass of the structure. So it can be written as follows [16]:

$$\mathrm{SEA(d)} = \frac{\mathrm{EA}(d)}{M} \tag{2}$$

where M is the mass of the structure. Apparently, the SEA is higher, the energy absorption capacity of a structure is better.

3 FINITE ELEMENT (FE) MODELING AND MATERIAL PROPERTIES

3.1 Material properties

The S-shape tube and the foam-filler structure are made of an aluminum extrusion AA6060-T4 with the following mechanical properties: Young's modulus $E = 68.2GPa$, initial yield stress $\sigma_y = 80MPa$, ultimate stress $\sigma_u = 173MPa$, Poisson's ratio $\mu = 0.3$ and mass density $\rho = 2.7\mathrm{x}10^3 kg/m^3$ [17]. In order to deal with this problem, the foam is divided into four different foam densities (0.3, 0.4, 0.5, and 0.6). Each density is considered as an isotropic uniform foam material whose constitutive behavior is based on as an isotropic uniform material model developed by Deshpande and Fleck [18].

Table 1. Material constants for aluminum foam.

	$\sigma_p(MPa)$	$\alpha_2(MPa)$	$1/\beta$	$\gamma(MPa)$	$E_p(MPa)$
$C_0(MPa)$	0	0	0.22	0	0
$C_1(MPa)$	720	140	320	42	$0.33\,\mathrm{x}\,10^6$
q	2.33	0.45	4.66	1.42	2.45

3.2 Finite element (FE) models

The FE model of the foam-filled S-shape tube is shown figure 2. The tube is modeled by using Belytschoko-Tsay four-node shell elements three integration points through the thickness and one integration point in the element plane. The foam-filler is meshed with eight-node solid elements with one-point reduced integration. An automatic node-to-surface contact is used to simulate the contact between the specimen and the rigid wall. An automatic single-surface contact is used to simulate the buckling of the foam-filler and the tube under axial dynamic loading.

In order to decide the size of elements, a convergence test was carried out to minimize the effect of mesh refinement on the accuracy of the numerical results. It is found that the optimal mesh sizes for the frame and foam-filler are 10×10 and 10×10×10 , respectively, as in figure 2, which was used through out the study. Figure 3 plots the kinetic, internal, total and hourglass energies during the deformation process of a foam-filled frame under dynamic loading. It is easily seen that the decrease in kinetic energy is almost equal to the increase of the internal energy, and the total energy remains nearly unchanged. The hourglass energy is less than 1% of the system internal energy. Note that the amount of hourglass energy is also a good indicator to estimate the mesh quality, which typically should be less than 5% of the internal energy of the system to overcome the hourglass problem [19]. Therefore, the mesh sizes used here are considered adequate to capture the crashing details of the foam filled S-shaped frame.

(a) (b) (c)

Figure 2. Finite element modeling of foam-filled SF: (a) Foam-filled tube, (b) tube and (c) Foam-filler.

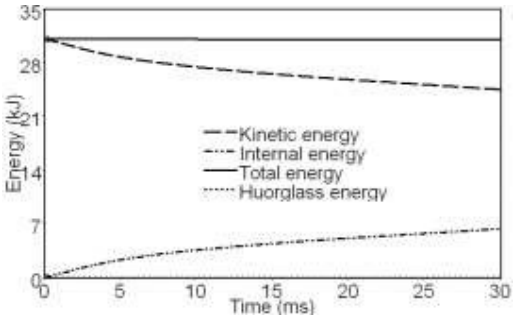

Figure 3. Kinetic, internal, total and hourglass energy of the foam-filled S-shape tube.

4 RESULTS AND DISCUSSION

4.1 Influence of the density on foam-filled S-shaped tube under various length of foam-filler

In the present work, a group of PFSTs and FFSTs with the same wall thickness (t = 2.5 mm) were compared for SEA and PCF. In each case, the deformation for calculating the energy absorption of foam-filled tube is chosen as 400 mm, which is about 50 percent of the total length of specimen. The foam-filled tubes with different parameters of L_f (420 mm, 540 mm, 660 mm, and 780 mm) and ρ_f (0.3, 0.4, 0.5, and 0.6 g/cm^3), which corresponding 16 different cases were adopted to explore the crashworthiness. Obviously, the full foam-filled tube is L_f equal to 780 mm (L_f is the duple distance from the outer side of the foam-filler to the center of frame in axial Z direction).

Figure 4 shows the effects of density foam and length foam-filler on the SEA and PCF of the PFSTs and FFSTs under axial dynamic loading. Fig. 4(a) plots the relationship between SEA and L_f with different foam densities, from which it can be seen that SEA of the PFSTs is greater than that of the corresponding FFSTs when L_f equal to 660 mm. However, an opposite result is observed when L_f equal to 420 mm. For the foam-filled tubes, obviously, parameter L_f and ρ_f has significant influence on SEA. Fig. 4(b) shows the relationship between the PCF and the length foam filler parameter L_f. The foam density has no influence on the PCF of PFST but it has significant influence on PCF of the FFST, which the PCF continuously increase as the foam density increasing. The maximum PCF of PFST is relatively lower than that of FFST counterpart.

The above observed crashworthiness characteristics of the S-shaped tubes can be further understood by looking at the final of different models of various length of foam-filler: L_f = 420 mm, 560 mm, 660 mm and 780 mm with the same foam-filler density of 0.5 as shown in Figure.5 (a), (b), (c) and (d), respectively. It is seen from the deformed shape in figure 5 that bending hinges is formed during collision process, except figure 5(c). As can be noted in figure 5(a) (b) shows a single local bending is observed in front and rear part of foam-filler. Figure 5(d), the plastic bending hinge has been occurred on the full foam-filled structure. Figure 5 (c) shows the effect of partial filling on configuration, as seen from the figure, the outward folds are formed on two straight parts of model and the major axial collapse is observed in the front and rear part of scheme.

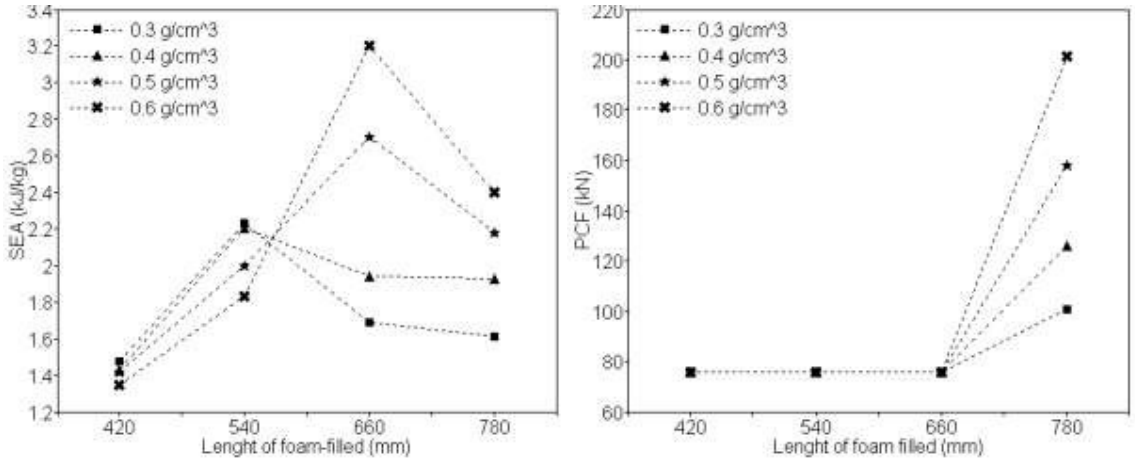

(a) (b)

Figure 4. Effect of foam density and length of foam filler on the structure response (a) SEA and (b) PCF.

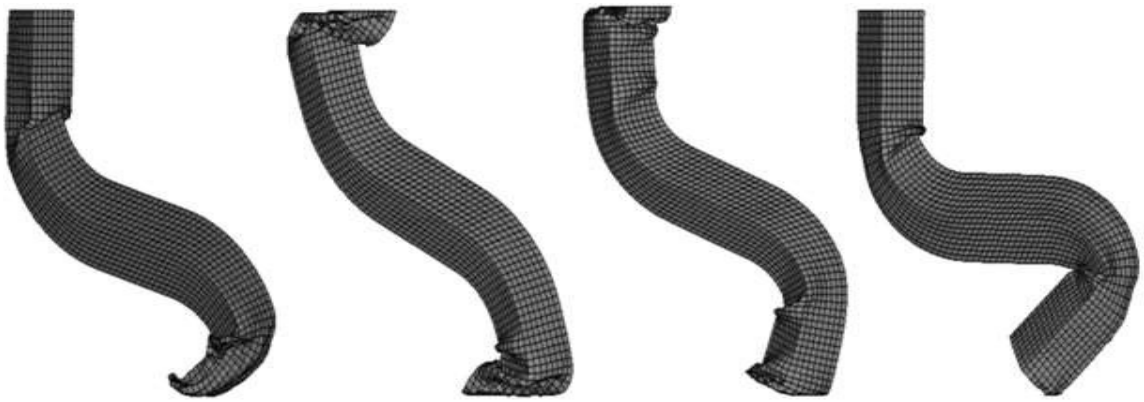

(a) (b) (c) (d)

Figure 5. Deformed shapes of the models with varying length of foam-filler with foam-filled density 0.5: (a) = 420 mm, (b) = 540 mm, (c) = 660 mm and (d) =780 mm.

4.2 Influence of the wall thickness on foam-filled S-shaped tube under various length of foam-filler

In this section, a group of PFSTs and FFSTs with the same density of foam-filler (ρ_f = 0.5) is evaluated. The foam-filled frames with different parameters of L_f (420 mm, 540 mm, 660 mm, and 780 mm) and t (1.5 mm, 2 mm, 2.5 mm, and 3 mm), which corresponding 16 different cases were adopted to explore the crashworthiness. Figure 6 shows the effects of wall thickness and length of foam-filler on the SEA and PCF of the PFSTs and FFSTs under axial dynamic loading. It is seen that for PFST, SEA continuously increases as the length of foam-filler increases for each wall thickness as seen from figure 6(a). While PCF continuously increases as the wall thickness increases for each length foam-filler as seen from figure 6(b). For FFSF, it is seen that both SEA and PCF continuously increase as the wall thickness increase.

Overall, the PFSTs have a better crashworthiness than the FFSTs in terms of SEA and PCF. Especially, these crashworthiness indicators of the PFST are superior when in around 660 mm. Therefore,

the PFST is a potential component in the crashworthiness design. Nevertheless, the variation in length of foam filler, foam density and wall thickness has a significant effect on crashworthiness of PFST. Therefore, it would be of great interest to seek best possible , and to optimize the crash characteristics of PFST.

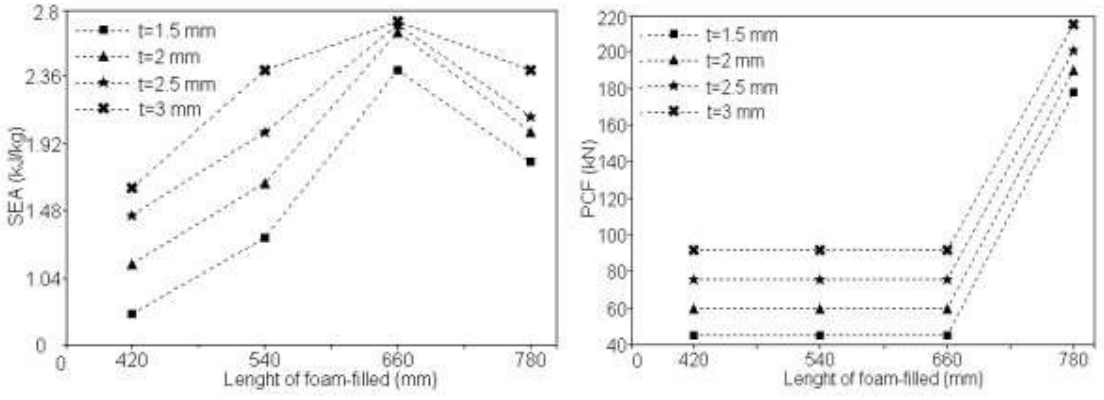

(a) (b)

Figure 6. Effect of wall thickness and length of foam filler on the structure response (a) SEA and (b) PCF.

5 MULTI-OBJECTIVE OPTIMIZATION DESIGN (MOD)

5.1 Methodology

As the main energy absorption component in the case of frontal impact, the foam-filled S-shape tube is expected to absorb as much kinetic energy as possible in case impact occurs. Thus, SEA should be chosen as an objective function and maximized in the crashworthiness optimization problem. One of other major concerns in crash is the peak force generation, which may determine structural integrity of vehicle and the occupant survival rate when impact occurs. An overly high PCF max often leads to severe injury or even death of occupant. Hence, these energy absorption components are also anticipated to have a minimum peak force. To account for these two different design criteria, the optimization problem can be written as the following multi-objective optimization form:

$$\text{for partial foam-filling} \begin{cases} Minimize\left[-\text{SEA}(t, L_f, \rho_f), \text{PCF}(t, L_f, \rho_f)\right] \\ S.t. \quad t^L \le t \le t^U \\ \qquad L_f^L \le L_f \le L_f^U \\ \qquad \rho_f^L \le \rho_f \le \rho_f^U \end{cases} \tag{3}$$

$$\text{for full foam-filling} \begin{cases} Minimize\left[-\text{SEA}(t, \rho_f), \text{PCF}(t, \rho_f)\right] \\ S.t. \quad t^L \le t \le t^U \\ \qquad \rho_f^L \le \rho_f \le \rho_f^U \end{cases} \tag{4}$$

where t, L_f and ρ_f is the wall thickness of structure, the length of foam-filler and the foam-filler density, respectively. $t^L - t^U$; $L_f^L - L_f^U$ and $\rho_f^L - \rho_f^U$ are the lower limit and upper limit of parameter t, L_f and ρ_f, respectively.

Design of experiment method provides a means of selection of the sampling points in the design space in a more efficient way. Many different experimental design methods can be used for sampling points in the design space [20, 21]. The full factorial design method is used to sample the design points in this paper for the advantage of its uniformity [22]. In this paper, for partial foam-filling, 64 (4×4×4) and for

full foam-filling, 16 (4×4) experimental design points are obtained using the full factorial design method for the design spaces of 1.5 to 3, 420 to 780 and 0.3 to 0.6 of the thickness tube, the length and the density of filled foam respectively.

Metamodels are usually used in the optimization problems in modern industry. In this study, the metamodels of the objective functions are constructed using polynomial functions [23, 24]. Based on the developed metamodels, the objective function values in the design space can be easily calculated.

5.2 Multi-objective optimization design of PFSTs and FFSTs

According to the methodology mentioned in section 5.1, the accuracies of different polynomial functions for the PFSTs and PFSTs with orders ranging from 2 to 4 are summarized in table 2. From table 2, it can be found that the 3th-order polynomial functions are the most accurate ones in most cases, respectively. The deviations between 3th order polynomial functions are very small. Apparently, it can be found that the 3th-order polynomial functions of SEA and PCF are accurate enough for the optimization design in engineering. Thus, for unity a 3th-order polynomial function is selected in the following optimization design. The metamodels of SEA and PCF are established as:

$$\begin{aligned}\mathrm{SEA}^{P} = {} & 14.9343 + t\,0.131633 - L_f\,0.08255 - \rho_f\,5.04924 + t^2\,0.686522 + L_f^2\,0.000144 - \rho_f^2\,21.1547 - tL_f\,0.00242 + \\ & L_f\rho_f\,0.050888 - \rho_f t\,1.46124 - t^3\,0.10283 - L_f^3\,7.90\mathrm{x}10^{-8} + \rho_f^3\,10.74979 - t^2 L_f\,4.10\mathrm{x}10^{-5} + t^2\rho_f\,0.017065 - \\ & L_f^2 t\,1.43\mathrm{x}10^{-7} - L_f^2\rho_f\,4.07\mathrm{x}10^{-5} + \rho_f^2 t\,0.526425 + \rho_f^2 L_f\,0.003609 - tL_f\rho_f\,0.003074\end{aligned} \tag{5}$$

$$\begin{aligned}\mathrm{PCF}^{P} = {} & -1813 - t\,14.6562 + L_f\,8.7346 + \rho_f\,2291.3020 + t^2\,7.0249 - L_f^2\,0.0136 - \rho_f^2\,1046.25 + tL_f\,0.1107 - L_f\rho_f\,7.1785 + \rho_f t\,1.2499 - \\ & t^3\,0.9999 + L_f^3\,6.9203\mathrm{x}10^{-6} + \rho_f^3\,354.1666 - t^2 L_f\,0.0012 + t^2\rho_f\,3 - L_f^2 t\,0.000085 + L_f^2\rho_f\,0.0059 + \rho_f^2 t\,2.5 + \rho_f^2 L_f\,1.125 - tL_f\rho_f\,0.0339\end{aligned} \tag{6}$$

for PFSTs and

$$\mathrm{SEA}^{F} = -0.7788 + t\,0.3698 + \rho_f\,10.2742 - t^2\,0.2555 + t\rho_f\,1.5520 - \rho_f^2\,22.1375 - t^3\,0.03 - t^2\,0.89 - \rho_f^2 t\,4.55 + \rho_f^3\,21.25 \tag{7}$$

$$\mathrm{PCF}^{F} = -144.6949 + t\,56.5699 + \rho_f\,874.9333 - t^2\,4.8999 - t\rho_f\,76.59999 - \rho_f^2\,1485 - t^3\,2.6169{*}10^{-10} + t^2\rho_f\,12 + \rho_f^2 t\,10 + \rho_f^3\,1416.7 \tag{8}$$

for FFSTs.

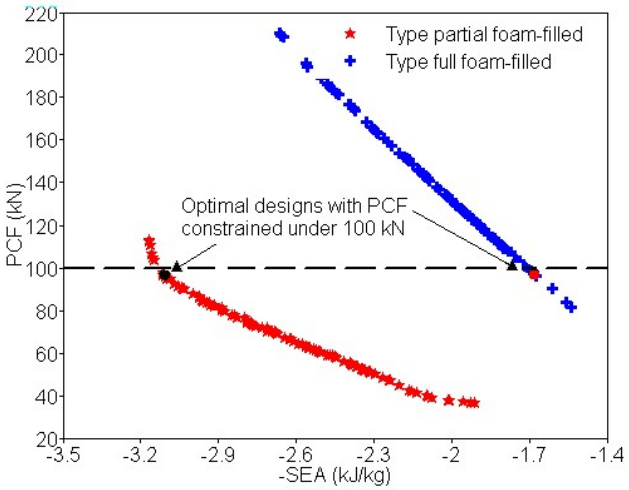

Figure. 7. Pareto fronts of the PFST and FFST.

Based on the metamodels, the Pareto fronts of the PFSTs and the FFSTs for the optimization problem defined as Eq. (5), (6), (7) and (8) are obtained and shown in figure 7 by using the MOPSO algorithm. It can be easily found that the Pareto front of PFSTs is more predominant than that of the FFSTs. In other words, the energy absorption capacity per unit mass of type PFSTs is better than that of the FFSTs when PCF is constrained under the same level. And the optimal designs (PCF constrained under 100 kN) to the

Pareto points of the PFSTs and FFSTs are marked as blackness circle red circle in figure 7, respectively. The detailed design parameters of these optimal designs are listed in table 3. Then, the finite element models for the optimal designs are established. The comparison between the FEA results and the approximate results are shown in Table 3. It can be found that the absolute errors are less 0.4%, which is acceptable in engineering design. The deformation profiles of these optimal designs compressed by 300 mm are shown in figure 8(a)-(b). The collapse mode of the PFST is distinctly different from that of the PFSF. The plastic bending hinge has been occurred on the fully foam-filling case, while the axial multiple-fold and axially collapsed shape are appeared on the partially foam-filling case. This explains why the PFSTs can absorb more energy than the FFSTs, but they also have PCF lower.

Table 2. Accuracies of the metamodels for the S-shape tube.

Metamodel		Order	R^2	RMSE	MAX	RE (%)
PFST	SEA	2	0.8957	6.8324	0.33	[-0.33,0.25]
		3	0.9518	5.1339	0.12	[-0.32,0.25]
		4	0.3529	56.488	0.94	[-5.7,4.8]
	PCF	2	0.8748	8.2895	31	[-0.75,0.33]
		3	0.9658	4.7886	8	[-0.16,0.19]
		4	0.2714	17.114	86	[-5.4,4.2]
FFST	SEA	2	0.982	0.063	0.11	[-0.9,0.4]
		3	0.994	0.0478	0.06	[0.12,0.16]
		4	0.96	8.068	3.24	[-2.4,5.2]
	PCF	2	0.999	1.448	1.78	[-1.7,0.8]
		3	0.999	0.719	0.71	[-0.27,0.2]
		4	0.72	5.87	9.9	[-1.4,8.3]

Table 3. Optimal solutions with PCF constrained under 100 kN.

	t (mm)	L_f (mm)	ρ_f (g/cm^3)	SEA (kJ/kg)			PCF (kN)		
				Metamodel	FEA	Error%	Metamodel	FEA	Error%
PFST	2.9	668	0.59	3.031	3.038	0.23	99.745	99.864	0.12
FFST	1.825	780	0.396	1.770	1.775	0.28	99.672	99.873	0.2

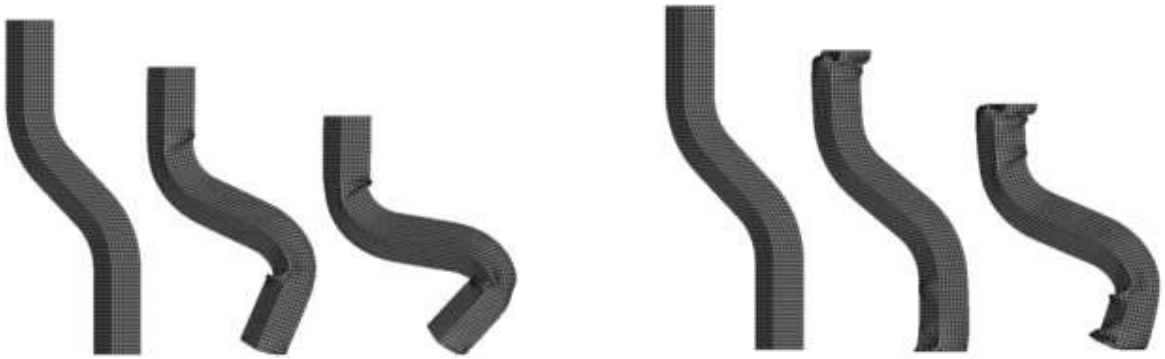

(a) FFST (b) PFST

Figure. 8. Deformed profiles at different stages of crushing process under axial dynamic loading of optimal designs with PCF constrained under 100 kN

6 CONCLUSION AND REMARKS

In this study, the partially and fully foam-filled S-shape square tube with 32 different types has been investigated under axial dynamic loading by using nonlinear finite element code LS-DYNA. The numerical results show that the peak crushing force of the FFST is higher than that of the PFST. It is also

found that the energy absorption capability per unit mass of the PFSTs is comparatively better than the FFSTs when in around 660 mm.

Then the multi-objective optimization using the multi-objective particle swarm optimization (MOPSO) algorithm has been presented for the both PFST and the FFST. The cubic polynomial functions of the SEA and PCF are the suitable matamodels for both PFST and FFST. By comparing the Pareto fronts of two kinds of foam-filling as partial and full foam, we fine that the energy absorption capability per unit mass of the PFSTs is more powerful than that of the FFSTs while the PCF constrained under the same level. This indicates the partially foam-filled S-shape tube is superior to the fully foam-filled S-shape tube in the cases considered.

REFERENCES

[1] E.M. Sobhan , P. Sadjad , E.M. Sareh, Crashworthiness Analysis of S-Shaped Structures Under Axial Impact Loading, Latin American Journal of Solids and Structures, ISSN 1679-7817On-line version ISSN 1679-782. 2017.

[2] K. Abolfazl, Optimal design of the S-rail family for an automotive platform with novel modifications on the product-family optimization process, Thin-Walled Structures 138(May 2019):Pages 143-154.

[3] C. Kefang, W. Dengfeng, Optimizing the design of automotive S-rail using grey relational analysis coupled with grey entropy measurement to improve crashworthiness, Structural and Multidisciplinary Optimization 56(12) · June 2017.

[4] H. Kim, T. Wierzbicki, Effect of the cross-sectional shape of hat-type cross sections on crash resistance of an S-frame. Thin-Walled Structures 2001;39:535-54.

[5] C. Zhang, A. Saigal, Crash behavior of a 3D S-shape space frame structure. Journal of Materials Processing Technology 2007;191:256-9.

[6] E. Ahmed, X. L. Yee, M. John. Crash analysis and energy absorption characteristics of S-shaped longitudinal members. Thin-Walled Structures 2013;68:55-74.

[7] M. Seitzberger, F. G. Rammerstorfer, H. P. Degiseher, R. Gradinger, Crushing of axially compressed steel tubes filled with aluminium foam. Acta Mech 1997;125(14):93105.

[8] A. Reyes, O. S. Hopperstad, A. G. Hanssen, M. Langseth, Modeling of material failure in foam-based components. International Journal of Impact Engineering 30 (7) (2004) 805-834.

[9] W. Chen, Wierzbicki, S. Santosa, Bending crush behavior of foam-filled sections, presented at the Int. Conf. on Metal Foams and Porous Metal Structures, Bremen Germany, June 14-16, 1999.

[10] H. R. Zarei, M. Kroger, Optimization of the foam-filled aluminum tubes for crush box application. Thin Wall Struct 2008;46 (2):214-21.

[11] H. R. Zarei, M. Kroger, Crashworthiness optimization of empty and filled aluminum crash boxes. Int J Crashworthines 2007;12(3):255-64.

[12] S. J. Hou, Q. Li, S.Y. Long, X.J. Yang, W. Li, Crashworthiness design for foam filled thin-wall structures. Mater Des 2009;30(6):2024-32.

[13] S. J. Hou, X. Han, G.Y. Sun, S. Y. Long, X. J. Yang, W. Li, et al. Multiobjective optimization for tapered circular tubes. Thin Wall Struct 2011;49(7):855-63.

[14] J. Bi, H. B. Fang, Q. Wang, X. C. Ren, Modeling and optimization of foam-fill walled columns for crashworthiness designs. Finite Elem Anal Des 2010;46(9):698-709.

[15] Y. Zhang, G. Y. Sun, G.Y. Li, Z. Luo, Q. Li, Optimization of foam-filled bitubal structures for crashworthiness criteria. Mater Des 2012;38:99-109.

[16] Kim H.S. New extruded multi-cell aluminum profile for maximum crash energy absorption and weight efficiency. Thin Wall Struct 2002;40(4):311-27.

[17] S.P. Santosa, T. Wierzbicki, A.G. Hanssen, Langseth Magnus. Experimentaland numerical studies of foam-filled sections. Int J Impact Eng 2000; 24(5):509-34.

[18] V.S. Deshpande, N.A. Fleck, Isotropic constitutive models for metallic foams. J Mech Phys Solids 2000; 48(6-7):1253-83.

[19] L. Mirfendereski, M. Salimi, Ziaei-Rad S (2008) Parametric study and numerical analysis of empty and foam-filled thin-walled tubes under static and dynamic loadings. Int J Mech Sci 50(6):1042-1057

[20] G. G. Wang, S. Shan, Review of metamodeling techniques in support of engineering design optimization. ASME Trans J Mech Des 2007;129(4):370-80.

[21] J.P.C. Kleijnen, An overview of the design and analysis of simulation experiments for sensitivity yanalysis. Eur J Oper Res 2005;164(2):287-300.

[22] S.J. Hou, Q. Li, S.Y. Long, X.J. Yang, W. Li, Multiobjective optimization of multi-cell sections for the crashworthiness design. Int J Impact Eng 2008;35(11):1167-355.

[23] H. Kurtaran, A. Eskandarian, D. Marzougui, Crashworthiness design optimization using successive response surface approximations. Comput Mech 2002; 29(45):409-21.

[24] J. Forsberg, L.Nilsson, Evaluation of response surface methodologies used in crashworthiness optimization. Int J Impact Eng 2006; 32(5):759-77.

THIẾT KẾ TỐI ƯU HÓA ỐNG HỘP VUÔNG HÌNH CHỮ S ĐƯỢC ĐIỀN BỌT NHÔM DƯỚI TẢI TRỌNG ĐỘNG LỰC HỌC

Tóm tắt. Bài viết trình bày mô phỏng phần tử hữu hạn về hành vi va chạm và đặc tính hấp thụ năng lượng của ống vuông hình chữ S được điền đầy hoặc một phần bọt nhôm. Dựa trên các kết quả mô phỏng số thấy rằng, mật độ, chiều dài của bọt nhôm điền trong ống và độ dày của ống có ảnh hưởng trực tiếp đến sự hấp thụ năng lượng lượng trên một đơn vị khối lượng (SEA) và lực tương tác cực đại (PCF) của các ống hình chữ S khi có va chạm. Trong bài báo này, giải thuật tối ưu hóa bầy đàn đa mục tiêu (MOPSO) được sử dụng để tìm ra ống hình chữ S chứa một phần bọt nhôm (PFSTs) và ống hình chữ S chứa đầy bọt nhôm (FFST) thông qua các thông số thiết kế khác nhau: mật độ, chiều dài của bọt nhôm điền vào ống và độ dày của ống, trong đó các mô hình bề mặt đáp ứng được thiết lập để tính toán SEA và PCF. Các kết quả tối ưu hóa cho thấy khả năng hấp thu năng lượng trên một đơn vị khối lượng của ống hình chữ S chứa một phần bọt nhôm có tiềm năng hơn ống hình chữ S chứa đầy bọt nhôm khi va chạm cùng một lực đỉnh.

Ngày nhận bài: 26/03/2019
Ngày chấp nhận đăng: 12/11/2019